AMD-Vol. 141
DSC-Vol. 37

DYNAMICS OF FLEXIBLE MULTIBODY SYSTEMS: THEORY AND EXPERIMENT

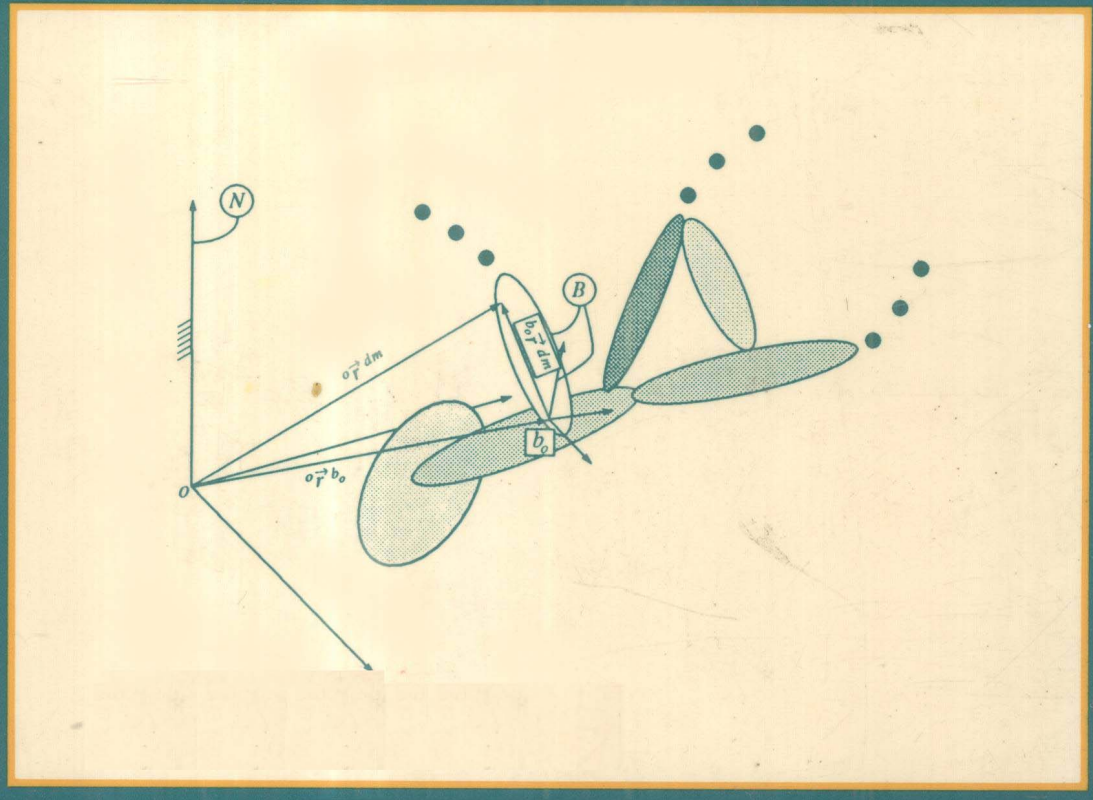

edited by
S. C. SINHA
H. B. WAITES
W. J. BOOK

AMD-Vol. 141
DSC-Vol. 37

DYNAMICS OF FLEXIBLE MULTIBODY SYSTEMS: THEORY AND EXPERIMENT

PRESENTED AT
THE WINTER ANNUAL MEETING OF
THE AMERICAN SOCIETY OF MECHANICAL ENGINEERS
ANAHEIM, CALIFORNIA
NOVEMBER 8–13, 1992

SPONSORED BY
THE APPLIED MECHANICS DIVISION AND
THE DYNAMIC SYSTEMS AND CONTROL DIVISION, ASME

EDITED BY
S. C. SINHA
AUBURN UNIVERSITY

H. B. WAITES
NASA, MARSHALL SPACE FLIGHT CENTER

W. J. BOOK
GEORGIA INSTITUTE OF TECHNOLOGY

THE AMERICAN SOCIETY OF MECHANICAL ENGINEERS
345 East 47th Street ■ United Engineering Center ■ New York, N.Y. 10017

ISBN No. 0-7918-1076-3

Library of Congress
Catalog Number 92-56539

FOREWORD

The study of dynamics and control of flexible multibody systems has become increasingly important in recent years due to the problems encountered in the design of proposed space stations, large spacecrafts, lightweight robots performing rapid maneuvers and machine components subjected to high speed operating conditions. In order to provide a forum for exchange of recent developments on the subject, the Applied Mechanics Division and the Dynamic Systems and Control Division of ASME jointly sponsored a symposium on "Dynamics of Flexible Multibody Systems: Theory and Experiment" at the Winter Annual Meeting held in Anaheim, California, November 8–13, 1992.

This book of proceedings contains all the twenty-seven papers presented in six sessions on November 12 and 13, 1992 at the symposium and covers various issues related to the problem of flexible multibody dynamics and control. The papers appear in the same order as they were presented.

A successful organization of a symposium is a considerable task, particularly for someone like myself who can hardly claim any expertise on this topic. First, I would like to thank all the authors for promptly submitting their valuable contributions and meeting the deadlines, some of which were not very convenient due to some reason or the other. I would also like to thank Professor Wayne Book, Professor Ahmed Shabana, and Dr. Ramen Singh for organizing various sessions for the symposium and Dr. Henry Waites for sharing the burden. Last, but not the least, my sincere thanks are due to Ms. Marilyn Swaim of the Mechanical Engineering Department, Auburn University for providing secretarial assistance and Ms. Barbara Signorelli at the ASME Headquarters for making sure of its publication on time.

S. C. Sinha
Auburn University

CONTENTS

AMD-Vol. 141/DSC-Vol. 37, Dynamics of Flexible Multibody Systems:
Theory and Experiment
ASME 1992

COOPERATIVE MANIPULATION OF FLEXIBLE OBJECTS: INITIAL EXPERIMENTS

David W. Meer and Stephen M. Rock
Aerospace Robotics Laboratory
Stanford University
Stanford, California

Abstract

The vast majority of the work done on multiple manipulator systems has focused on manipulating rigid objects, both in free-space motion and contact tasks. Not all objects encountered in potential robotic applications are rigid, however. Spring-loaded parts, lightweight space structure members, and heavy cabling provide just a few examples of flexible objects that robots may need to manipulate in the future.

This paper presents a testbed for the study of cooperative manipulation of flexible objects. It discusses some of the important characteristics required for this study. Using this testbed, the limitations of two control strategies used for manipulation of rigid objects are demonstrated when applied to flexible objects. The results justify the validity of the testbed as well as providing motivation for further study.

Introduction

The advantages of using multiple manipulators include increased payload capability, improved dexterity with larger objects, and expanded functionality. Most previous research, however, focused on developing control strategies for multiple robotic arms manipulating a single, rigid body. What happens when the manipulated object is flexible? Various potential robotic applications, from the assembly of spring loaded parts in a manufacturing environment to the servicing of satellite solar arrays in orbit, will involve the manipulation of flexible objects by multiple manipulators.

One of the most promising and general approaches to cooperative manipulation is object-level control. This technique allows the operator to issue task level commands, such as "capture this object" or "insert this connector into that fixture". The controller takes care of the details of the operation, drawing upon a library of task primitives, freeing the user to perform other tasks. This capability has been developed and demonstrated successfully on a wide variety of experimental platforms. [1] [2] [3]

The goal of this research is to extend object-level control to flexible objects. This paper presents some preliminary findings. First, an experimental testbed is described. It consists of a pair of arms and a flexible object. Next, two attempts to apply previously developed control strategies to a flexible object using this experimental testbed are discussed. The first, Object Impedance Control (OIC), developed for cooperative manipulation of rigid objects, performed poorly in attempts to regulate the free space motion of the object. In fact, this controller was unstable for higher object stiffnesses. The second control strategy, a coordinated PD control, was stable and could perform free space manipulations without undue excitation of the object's flexibility. The coordinated PD controller, however, proved insufficient for tasks involving deformation of the object. These results show that current controllers, designed for manipulation of rigid objects, perform poorly when applied to a flexible object and that the experimental testbed embodies the problem of interest.

Related Work

Some work has been done on the control of flexible objects with robotic manipulators. This body of work addresses various aspects of the problem, including trajectories and task formulation. It does not, however, focus on the interaction between the flexibility and the controller.

Zheng and Luh [4] used a flexible object to eliminate kinematic redundancy problems in their early work on coordinated control of multiple manipulators. These results seem to indicate that, in some cases, flexibility in the object may make the task of controlling such systems easier.

Recently, Dauchez, et al, presented experimental results for a pair of 6 dof arms deforming a spring and transporting the spring in the deformed state [5]. They used symmetric hybrid position/force control. The principal contribution of the work was the method they used to describe the task with "virtual sticks".The algorithm used, however, was so computationally complex that the controller ran at 20 Hz. Also, the hybrid control approach requires task dependent control mode switching. This can be a disadvantage when performing complex tasks.

Zheng, Pei, and Chen [6] have also done work on assembly of deformable objects. The assemblies involved sliding a long, flexible beam into a hole with a single manipulator. The principal contribution of this work was determining the proper trajectory for the arm to follow based upon the beam properties and the tightness of fit.

The goal of this research is to explore the interaction between object flexibility and the system controller.

Design Objectives

Several criteria helped shape the design of the experimental apparatus used to study cooperative manipulation of flexible objects. First, the arms should be as "ideal" as possible. An "ideal" arm would produce specified forces and accelerations at the endpoint exactly. This allows the experiments to focus on the problems introduced by flexibility in the object rather than those caused by friction at the robot joints, flexibility in the drive train, etc. The goals in designing the flexible object included (1) introducing the flexibility at a frequency of interest within the bandwidth of the control system, (2) providing the capability to change the natural frequency and stiffness of the flexible element in order to study the effect of varying these parameters, and (3) creating an object that was deformable with the available actuators in order to study assembly operations requiring deformation of the object. Finally, the testbed should not be so geometrically complex that the computational speed of the control computers severely limits the algorithms that can be applied to the system.

Experimental Apparatus

Addressing the last of the design criteria, the experimental testbed is limited to 2 dimensions, simplifying the computational complexity significantly. The flexible object has 4 degrees of freedom (DOF) and each manipulator has 2 DOF. The flexible object floats on air bearings over a granite surface plate, eliminating the effects of gravity on the system and simulating the drag-free environment of space. These simplifications enable the research to focus on the problem of interest: how flexibility affects the control of an object grasped by multiple manipulators.

Cooperating Manipulators

Figure 1 depicts one of the pair of experimental arms. Each manipulator is a direct-drive, SCARA two-link arm, with revolute "shoulder" and "elbow" joints. At the tip of each arm is a two-dimensional force sensing pneumatic gripper. These grippers fit into ports on the manipulation objects. The connection is mounted on a bearing pin joint, so the manipulator cannot apply torque at the connection. The system thus provides frictionless two-dimensional motion.

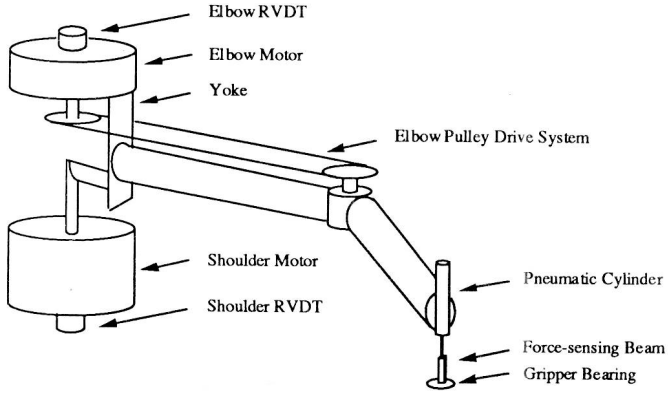

Figure 1: **Arm Schematic**

A schematic view of one of the two link, SCARA, arms used in the experimental testbed.

The manipulators have a reach of 0.65 meters and are separated by 0.60 meters at the shoulder hub. The motors on the manipulator are DC limited-angle torquers. A motor located at the shoulder transmits torque to the elbow joint through a steel cable. Joint angles are measured by a rotary variable differential transformer (RVDT) mounted on each motor shaft. Each arm also has a vision target located over the gripper for use with an overhead vision system. See [7] for a detailed description of the manipulators.

Many factors, including the direct drive nature of the arms, the vision and force sensors at the endpoint, the two dimensional nature of the experimental system that eliminates the need for gravity compensation, and accurate calibration of the motors bring these manipulators close to the "ideal".

Flexible Object

The flexible object consists of two pads that float on an air cushion over the granite surface plate. These pads are joined by a six bar linkage. The linkage is designed to add a single flexible degree of freedom to the object. Figure 2 shows the object in both the nominal configuration (solid lines) and the deformed configuration (dashed lines). The circles represent pin joints in the mechanism while the thicker lines show the two sections of steel wire that give the object its flexibility. These segments can easily be switched out to change the stiffness of the flexibility in the object. Each pad also has two gripper ports and a target for tracking by the overhead vision system (not shown in the drawing).

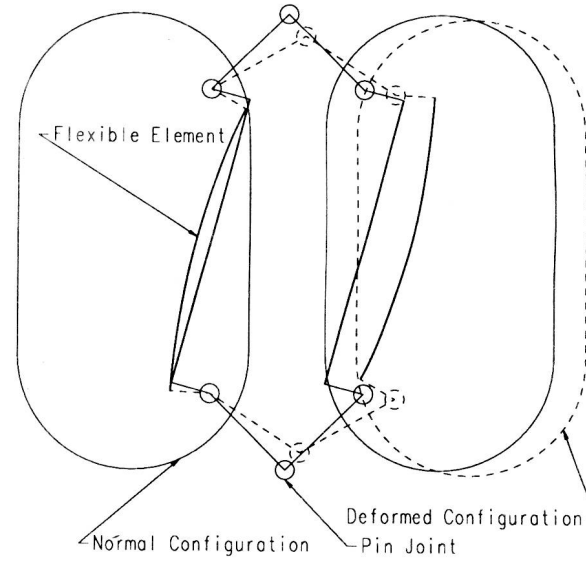

Figure 2: **Flexible Object**

This flexible object, which floats on a granite surface plate, uses a six bar mechanism with 2 flexible elements. The object thus has three rigid degrees of freedom and one flexible degree of freedom.

As Figure 3 shows, the free vibration of the flexible object, with the particular stiffness used in these initial experiments, has a natural frequency of 3.06 Hertz. This plot also shows the very lightly damped characteristic of the linkage. The linkage gives the object a range for the distance between the pads of between .025 meters and .09 meters, with a nominal separation of .064 meters.

Current Control Strategies

This section briefly outlines the two control strategies applied to the experimental system. The motivation for these experiments was to demonstrate that deficiencies exist with current control strategies when applied to flexible objects and to test the validity of the experimental testbed.

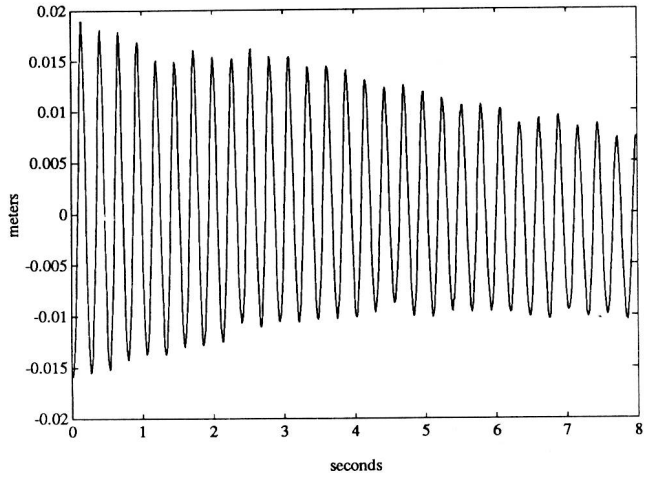

Figure 3: **Free Vibration of Flexible Object**

This plot shows the deflection from the nominal separation of the two pads of the flexible object for a nonzero initial condition. Note the lightly damped response.

Object Impedance Control

The Object Impedance Control (OIC) strategy enforces a controlled impedance of the manipulated object [8]. Equation 1 contains the particular impedance relationship chosen for this controller.

$$m_d(\ddot{x} - \ddot{x}_{des}) + k_v(\dot{x} - \dot{x}_{des}) + k_p(x - x_{des}) = f_{ext} \quad (1)$$

Here, x is the coordinate of any one DOF of an arbitrary frame fixed relative to the object's frame. The constants m_d, k_p, and k_v can be specified independently for each degree of freedom. x_{des} represents the desired position of the chosen frame and $\ddot{x}_{des}$ is acceleration feedforward. The derivation of the control equations based on the desired object behavior specified in Equation 1 is fully contained in Schneider [8]. Basically, the controller attempts to cancel the actual object dynamics and make the object behave according to Equation 1. This produces a desired acceleration, $\ddot{x}_{des}$, and force, f_{des}, at each arm endpoint. Then, if M and J represent the mass matrix and Jacobian for a given arm and q is the vector of joint angles, the arm kinematics yield:

$$\ddot{q}_{des} = J^{-1}(\ddot{x}_{des} - \dot{J}\dot{q}) \quad (2)$$

Combining this with the arm equations of motion, where C contains the nonlinear coriolis and centrifugal terms,

$$\tau = M\ddot{q}_{des} + C(q, \dot{q}) + J^T f_{des} \quad (3)$$

produces the desired torques for each arm, τ. These equations are for the simplified planar case.

This technique requires an accurate model of the dynamic behavior of the object. It also uses the location of the object in the feedback loop. Endpoint feedback techniques are generally not very robust to the introduction of unmodelled modes of vibration. Consequently, the unmodified Object Impedance Controller applied to a flexible object was expected to perform poorly.

Object PD Control

The second control strategy tested was a very simple coordinated PD control. Coordinated control refers to an approach that uses the desired motion of the center of mass of the object to calculate the desired motion of the the grip points. This control makes no attempt to compensate for dynamic forces, relying on the strictly kinematic relationship between the grip points and the object center of mass. This approach treats the arms as a simple force source, calculating the force that each arm should apply using a PD control law on the gripper port. This yields

$$f_{arm} = k_p(p_{des} - p) + k_v(\dot{p}_{des} - \dot{p}) \quad (4)$$

where f_{arm} is the desired arm endpoint force, k_p and k_v are specifiable position and velocity gains, p represents the endpoint position of the arm, and p_{des} is the desired arm endpoint location. The desired arm endpoint location, p_{des}, comes from the kinematic relationship between the desired object center of mass and the grip point on the object. The controller simply runs the desired endpoint force, f_{arm}, through the Jacobian, J, to produce the torques at the joints, τ.

$$\tau = J^T f_{arm} \quad (5)$$

This control should be stable regardless of the object's dynamics, since it essentially treats the motion of the object, including the flexibility, as a disturbance to the arm endpoint.

Experimental Results

Object Impedance Control

Experimentally, the Object Impedance Control strategy proved unstable for motions that provided sufficient excitation to the flexible object. Figure 4 shows a time history of the spring mechanism compression for a slew of 0.15 meters in 1.0 seconds in the upper plot. The lower plot shows the desired and actual center of mass X position. The slew begins at about 1.5 seconds. Clearly, the interaction between the object's flexibility and the controller is leading to instability. Also note that, despite the excitation of the flexibility, the object's X position does not deviate significantly from the desired.

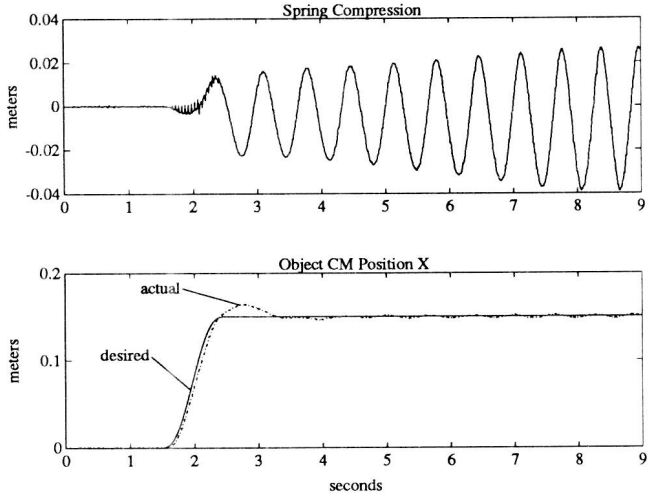

Figure 4: **Object Impedance Slew**

As this plot of the spring compression during a slew shows, the Object Impedance Controller can excite the flexible mode in the object.

Object PD Control

As Figure 5 shows, the gripper point PD controller was stable for the same slew that caused the object impedance controller to go unstable.

So, the simple PD controller works well for free space motions. While the flexibility was excited somewhat, the PD controller quickly damped it out once it began regulation.

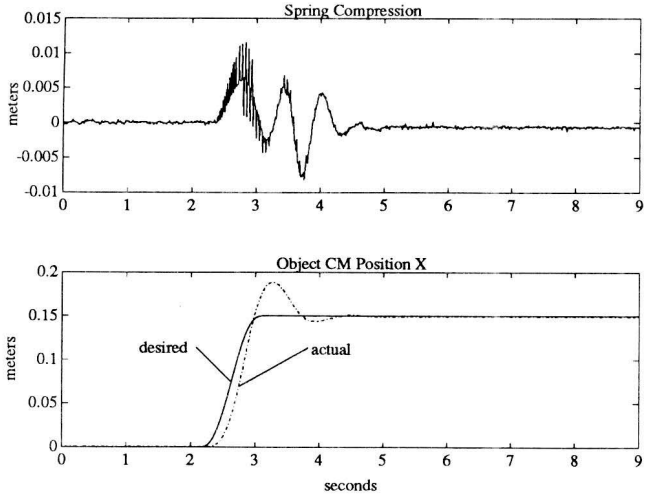

Figure 5: **PD Slew**

While the PD controller applied to the flexible object exhibits significant overshoot, it does damp out any excitation of the flexibility.

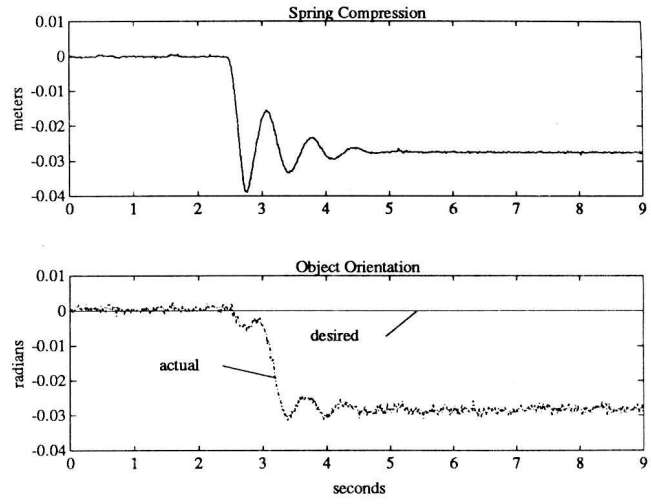

Figure 6: **PD Spring Compression**

When commanded to deform the flexible object, the PD controller rotated the object as well as compressing it.

The next test involved directly manipulating the flexibility in the object. Figure 6 shows the distance between the ports for a desired compression of -0.12 meters beginning at about 2.5 seconds. The actual compression achieved, -0.0275 meters in this case, depends upon the proportional gains used in the controller. Also note that the object rotates as it compresses. So, while this simple coordinated PD controller can damp out the object vibrations when the spring is unstretched, it does not control the object adequately for manipulations involving deformation.

Conclusions

This paper describes a hardware testbed developed to study the problem of manipulation of flexible objects. It discusses the criteria used to design a testbed to study the problem of interaction between the system controller and the flexibility in the object. A flexible object composed of two rigid bodies coupled by a mechanism designed to be flexible in one dimension is the principal difference between this system and systems studied in previous work. To validate the testbed and demonstrate that a problem does exist, two controllers were applied to the experimental system. For the first strategy, Object Impedance Control, the results demonstrated a sensitivity to modelling error. The controller performed marginally, at best, and sometimes proved unstable, depending upon the stiffness of the object. The second approach, a coordinated PD controller was stable and did exhibit reasonable performance in free motion. However, it did a poor job of controlling the object for tasks that involved deformation.

References

[1] S. Schneider and R. H. Cannon. Experiments in cooperative manipulation: A system perspective. In *Proceedings of the NASA Conference on Space Telerobotics*, Pasadena, CA, February 1989. NASA.

[2] M. A. Ullman. *Experiments in Autonomous Navigation and Control of Multi-Manipulator Free-Flying Space Robots.* PhD thesis, Stanford University, Stanford, CA 94305, (February) 1992. To be published.

[3] Lawrence Pfeffer. *Experiments in Control of Cooperating, Flexible Robotic Manipulators.* PhD thesis, Stanford University, Stanford, CA 94305, (March) 1992. To Be Published.

[4] Y. F. Zheng, J. Y. S. Luh, and P. F. Jia. A real-time distributed computer system for coordinated motion control of two industrial robots. In *Proceedings of the International Conference on Robotics and Automation*, pages 1236–1241, Raleigh, NC, April 1987. IEEE.

[5] Pierre Dauchez, Xavier Delebaree, Yann Bouffard, and Eric Degoulange. Task description for two cooperative manipulators. In *Proceedings of the American Control Conference*, pages 2503–2508, Boston, MA, June 1991. IEEE.

[6] Yuan F. Zheng, Run Pei, and Chichyang Chen. Strategies for automatic assembly of deformable objects. In *Proceedings of the International Conference on Robotics and Automation*, pages 2598–2603, Sacramento, CA, April 1991. IEEE.

[7] S. Schneider. *Experiments in the Dynamic and Strategic Control of Cooperating Manipulators.* PhD thesis, Stanford University, Stanford, CA 94305, September 1989. Also published as SUDAAR 586.

[8] S. Schneider and R. H. Cannon. Object impedance control for cooperative manipulation: Theory and experimental results. *IEEE Journal of Robotics and Automation*, 8(3), June 1992. Paper number B90145.

AMD-Vol. 141/DSC-Vol. 37, Dynamics of Flexible Multibody Systems:
Theory and Experiment
ASME 1992

NUMERICAL ANALYSIS OF NONMINIMUM PHASE ZERO FOR NONUNIFORM LINK DESIGN

Douglas L. Girvin and Wayne J. Book
George W. Woodruff School of Mechanical Engineering
Georgia Institute of Technology
Atlanta, Georgia

ABSTRACT

As the demand for light-weight robots that can operate in a large workspace increases, the structural flexibility of the links becomes more of an issue in control . When the objective is to accurately position the tip while the robot is actuated at the base, the system is nonminimum phase. One important characteristic of nonminimum phase systems is system zeros in the right half of the Laplace plane. The ability to pick the location of these nonminimum phase zeros would give the designer a new freedom similar to pole placement.

This research targets a single-link manipulator operating in the horizontal plane and modeled as a Euler-Bernoulli beam with pinned-free end conditions. Using transfer matrix theory, one can consider link designs that have variable cross-sections along the length of the beam. A FORTRAN program was developed to determine the location of poles and zeros given the system model. The program was used to confirm previous research on nonminimum phase systems, and develop a relationship for designing linearly tapered links. The method allows the designer to choose the location of the first pole and zero and then defines the appropriate taper to match the desired locations. With the pole and zero location fixed, the designer can independently change the link's moment of inertia about its axis of rotation by adjusting the height of the beam. These results can be applied to inverse dynamic algorithms currently under development at Georgia Tech and elsewhere.

INTRODUCTION

Controller design for collocated systems has been heavily researched and is well understood compared to controller design for noncollocated systems. In noncollocated systems, uncertainties from model inaccuracies and modal truncation present fundamental problems with system performance and stability [18]. The fundamental difference between collocated and noncollocated systems is the presence of these RHP zeros. To advance controller design for noncollocated systems, research needs to be conducted into the factors that affect the location of these RHP zeros. This research targets the relationship between RHP zeros and structural design.

Although research on RHP zeros is limited, there has been some notable research done in the past. In 1988, Nebot and Brubaker [13] experimented with a single-link flexible manipulator. In 1989, Spector and Flashner [19] investigated the sensitivity effects of structural models for noncollocated control systems. In 1990, Spector and Flashner [18] again studied modeling and design implications pertinent to noncollocated control. Also in 1990, Park and Asada [15],[14] investigated a minimum phase flexible arm with a torque actuation mechanism. In 1991, Park, Asada, and Rai [1] expanded their previous work on a minimum phase flexible arm with a torque transmission device.

The underlying issue in noncollocated control is how to deal with the RHP zeros in the control algorithm. A major step in solving the problem is understanding what design parameters can be used to change the location of these RHP zeros. This research targets the relationship between RHP zero location and structural design. Specifically, how do changes in the shape of the structure (link) affect the location of these zeros?

Traditionally links are designed with uniform properties along the length because analytic solutions to this problem exist. A link with variable cross-section cannot be solved analytically, but with aid of a computer a numerical approximation can be found. The key to an accurate numerical solution is a good model of the system.

The research presented in this paper models a single-link flexible rotary manipulator as a pinned-free beam. Transfer matrix theory was used to generate a beam with variable cross-section. FORTRAN code was written to generate the model and evaluate the system for the location of RHP zeros. The program was used to examine the relationship between link shape and RHP zero location. This

relationship can be directly applied to controller design using the inverse dynamics approach researched at Georgia Tech and elsewhere.

TRANSFER MATRIX THEORY

Transfer matrices describe the interaction between two serially connected elements. These elements can be beams, springs, rotary joints, or many others. In 1979 Book, Majette, and Ma [6] and Book [4] (1974) used transfer matrices to develop an analysis package for flexible manipulators. They used transfer matrices to serially connect different types of elements to model the desired manipulator. Of interest in this paper is how to connect similar types of transfer matrices (beam elements) to model a beam with different cross-sectional area. Pestel and Leckie [16] provide an in depth discussion of transfer matrix derivations and applications.

Transfer matrices can be mathematically expressed by Equation 3.1. The state vector u_i is given by the state vector u_{i-1} multiplied by the transfer matrix B.

$$u_i = [B_i]u_{i-1} \tag{3.1}$$

When elements are connected serially, the states at the interface of two elements must be equal. By ordered multiplication of the transfer matrices, intermediate states can be eliminated to determine the transfer matrix for the overall system.

The concept of state vector in transfer matrix theory is not to be confused with the state space form of modern control theory. The state equation in modern control theory relates the states of the system as a function of time. In transfer matrix theory the state equation relates the states at various points along the serial chain of elements. The independent variable in a transfer matrix is the Laplace or Fourier variable with units of frequency, not time. The elements of the matrix B depend on the frequency variable and therefore the states will change as the system frequency changes. The transfer matrix B essentially contains the (Laplace or Fourier) transformed dynamic equations of motion that govern the element in analytic form. Therefore, analytical solution of the transfer matrix alone does not involve numerical approximations to the partial differential equation modelling the beam. This is desirable since numerical approximations introduce error into the solution.

A single-link manipulator as pictured in Figure 3.1 can be thought of as a beam with torque applied at one end and free at the other end. There are several steps to determine the RHP zeros and imaginary poles of this system. First, develop a model for the beam. Second, determine the appropriate boundary conditions. Third, determine the system input and output. Fourth, solve for the system zeros. The following sections will discuss each of these steps in more detail.

A link with nonuniform cross-sections can be modeled as a series of discrete elements. While the shape of these elements is similar, the size can vary to allow for changes in cross-section. The appropriate element to model a flexible link is an Euler-Bernoulli beam element. The Euler-Bernoulli model neglects the effects of rotary inertia and shear deformation in the element. [11]. This assumption is generally valid for modeling beams whose length is roughly ten times the thickness. Flexible manipulators have long, slender links which are appropriately modeled under the Euler-Bernoulli assumption.

Transfer matrices are derived from the equation of motion for a given element. For a uniform Euler-Bernoulli beam element, the equation of motion transformed to the frequency domain has the form:

$$\frac{d^4w(x,\omega)}{dx^4} = \frac{\mu\omega^2}{EI}\, w(x,\omega)$$

where,

μ = mass density per unit length

ω = frequency in radians/second

E = Young's modulus

I = Cross sectional area moment of inertia

Notice the equation is fourth order thus requiring four states to describe the solution in transfer matrix form. The state vector for the Euler-Bernoulli element is:

$$u = \begin{bmatrix} -w \\ \psi \\ M \\ V \end{bmatrix} = \begin{bmatrix} \textit{displacement} \\ \textit{slope} \\ \textit{moment} \\ \textit{shear force} \end{bmatrix} \tag{3.3}$$

The first two elements of the state vector are displacements (w and ψ) while the last two elements are forces (V and M). This arrangement of states is characteristic of transfer matrix theory.

An analytic solution to Equation 3.2 can be found when the element has uniform properties (ie. constant cross-section, mass density, and stiffness). Equation 3.4 gives the transfer matrix for a uniform Euler-Bernoulli element. Each element of Equation 3.4 is a function of frequency and must be reevaluated as the frequency of interest changes.

$$TM = \begin{bmatrix} C_0 & lC_1 & aC_2 & alC_3 \\ \dfrac{\beta^4 C_3}{l} & C_0 & \dfrac{aC_1}{l} & aC_2 \\ \dfrac{\beta^4 C_2}{a} & \dfrac{\beta^4 lC_3}{a} & C_0 & lC_1 \\ \dfrac{\beta^4 C_1}{al} & \dfrac{\beta^4 C_2}{a} & \dfrac{\beta^4 C_3}{l} & C_0 \end{bmatrix} \tag{3.4}$$

where,

$$C_0 = \frac{1}{2}(\cosh\beta + \cos\beta) \quad (3.5)$$

$$C_1 = \frac{1}{2\beta}(\sinh\beta + \sin\beta) \quad (3.6)$$

$$C_2 = \frac{1}{2\beta^2}(\cosh\beta - \cos\beta) \quad (3.7)$$

$$C_3 = \frac{1}{2\beta^3}(\sinh\beta - \sin\beta) \quad (3.8)$$

and

$$\beta^4 = \frac{\omega^2 l^4 \mu}{EI} \quad (3.9) \qquad a = \frac{l^2}{EI} \quad (3.10)$$

With the transfer matrix for the fundamental beam elements, one can combine these elements serially to generate a model for the link. Figure 3.3 illustrates how a simple model can be constructed for a tapered beam. Although only two elements are considered here, more elements can be added to better approximate the shape of the link. Since the states at interface u_1 are the same for both elements, u_1 can be eliminated to obtain an overall transfer matrix for the beam:

$$u_2 = [B_2][B_1]u_0 \quad (3.13)$$

Eliminating one state simply illustrates the point that this multiplication can be carried out to eliminate all intermediate states in a model with more elements.

As previously mentioned, transfer matrices themselves are not numerical approximations. The transfer matrix for a Euler-Bernoulli beam contains the analytic solution for a uniform beam element. It is not an assumed modes solution. The approximation made in using transfer matrix theory involves the modeling of the beam and solution of the equations. To generate the model of a link with variable cross-section, the size of the elements must vary. The interface of two different size elements will be discontinuous. In Figure 3.3, interface 1 is discontinuous between elements A and B. These discontinuities are the major approximation when using transfer matrices to model a beam. This approximation can be minimized by using more elements to model a nonuniform beam. As more elements are added to the model, the discontinuities between elements will decrease thus reducing the effects of this approximation on the results.

Transfer matrix theory as used to represent a variable cross section is similar to Finite Element Analysis (FEA). In FEA, first the system must be discretized. Then an appropriate interpolation function must be selected to describe each element (ie. element stiffness). Next the system matrices must be assembled to produce a set of linear algebraic equations. Finally the linear equations are solved to get an approximate solution to the system under consideration. These boundary conditions are applied to the overall transfer matrix for the system and the appropriate state variables are set to zero.

$$\begin{bmatrix} -w \\ \psi \\ 0 \\ 0 \end{bmatrix}_{x=L} = \begin{bmatrix} B_{11} & \cdots & B_{14} \\ \vdots & \ddots & \vdots \\ B_{41} & \cdots & B_{44} \end{bmatrix} \begin{bmatrix} 0 \\ \psi \\ 0 \\ V \end{bmatrix}_{x=0} \quad (3.14)$$

Since this research targets the location of RHP zeros the system output is tip position, and the system input is joint torque. Considering the system input and output, the overall system transfer matrix will have the form:

$$\begin{bmatrix} -w \\ \psi \\ 0 \\ 0 \end{bmatrix}_{x=L} = \begin{bmatrix} B_{11} & \cdots & B_{14} \\ \vdots & \ddots & \vdots \\ B_{41} & \cdots & B_{44} \end{bmatrix} \begin{bmatrix} 0 \\ \psi \\ \tau \\ V \end{bmatrix}_{x=0} \quad (3.15)$$

In the above equation, w_L is the system output which corresponds to tip position, and τ is the system input corresponding to joint torque at the base of the manipulator.

With the system input and output chosen, Equation 3.15 can be simplified to relate system input to system output:

$$N = B_{12}B_{44}B_{33} - B_{12}B_{34}B_{43} + B_{13}B_{34}B_{42} - B_{13}B_{44}B_{32} + B_{14}B_{43}B_{32} - B_{14}B_{33}B_{42}$$

$$w_L = -\frac{N}{B_{34}B_{42} - B_{44}B_{32}} \quad (3.16)$$

Where B_{ij} are elements of the overall transfer matrix in Equation 3.15. When the frequency is found which renders the function inside the brackets zero the output at that frequency will always be zero regardless of the input; therefore, the zeros of the bracketed term are the system zeros.

To search for RHP zeros, one must consider what type of frequency to input into Equation (3.16). Using the relationship which defines the Laplace variable, s

$$s = j\omega \quad (3.17)$$

one can easily determine ω should have the form:

$$\omega = 0 - jb \qquad where \quad 0 \le b \le \infty \quad (3.18)$$

That is, imaginary negative values of ω will result in purely real positive values of s. Thus searching Equation 3.16 with frequencies of the form of Equation 3.17 one can find the location of the RHP zeros on the real axis.

Although the location of RHP zeros is of primary concern in this research, knowledge of pole location will help in analysis of the results. Since the system damping is ignored, the poles will lie on the imaginary axis of the s-plane in complex conjugate pairs. The location of these poles can be determined by simply searching the positive imaginary axis of the s-plane. Considering the applied boundary conditions, one can extract two homogeneous equations from Equation 3.14 to get the homogeneous system:

$$\begin{Bmatrix} 0 \\ 0 \end{Bmatrix} = \begin{bmatrix} B_{32} & B_{34} \\ B_{42} & B_{44} \end{bmatrix} \begin{Bmatrix} \psi \\ V \end{Bmatrix} \tag{3.19}$$

The poles (eigenvalues) of the system are those values of ω which make the determinant of the sub-transfer matrix in Equation 3.19 equal to zero (see reference [6] for a detailed explanation). For a two by two matrix this determinant is simply:

$$g(\omega) = B_{32}B_{44} - B_{34}B_{42} \tag{3.20}$$

Referring to Equation 3.17, one finds that Equation 3.20 is the denominator of the input/output transfer function which is to be expected. To find the values of the purely complex poles, one must search Equation 3.20 for its roots. According to the definition of s, ω must have the form:

$$\omega = b + j0 \tag{3.21}$$

Searching over a range of values for b will give the poles in that range. With the zero and natural frequency functions determined, the problem remains to implement a computer solution to find the RHP zeros and imaginary poles.

RESULTS

Unless otherwise specified, several dimensions remain the same from one study to the next (referred to as nominal dimensions). The overall length of the beams is 40 inches, and the height (which remains constant over length) is 1 inch. The material properties are selected to be those of aluminum: modulus of elasticity, E, is 10E6 psi, and the density is 9.55E-2 lbm/in^3.

Although the model was limited to uniform elements, there were any number of combinations one can find to represent the system. This study examined two different methods for modeling a linearly tapered beam. As shown in Figure 4.1 the link was tapered along the length in the width dimension while the height was held constant. The taper was described by two dimensions: the width at the base, A, and the width at the tip, B. The degree of taper, R=A/B, was used to compare different designs.

Using Method 1 to model the tapered link, the beam was divided into elements of equal length. For a three element model with length L, each element will have length L/3. The height of each element was the same, while the width of each element changed linearly as a function of x. Figure 4.2 presents modeling Method 1.

Using Method 2 to model the tapered link, the beam was divided into elements so the first and last element have length one-half of the intermediate elements. For a three element model with length L, the first and last elements will have length L/4 and the middle element will have length L/2. Again the height of each element was the same, while the width of each element changed linearly as a function of x. Figure 4.3 presents modeling Method 2.

Figures 4.2 and 4.3 illustrate the main difference between the two modeling methods. Method 2 compensated the elements at each end for meeting the specified end widths A and B. In both methods the width of intermediate elements was determined by the width of the tapered beam at the midpoint of each element. Since the end elements meet the specified A and B, the tapered link will not pass through the midpoint of these two elements. Method 2 compensates for this exception by making the end element lengths one half the length of the other elements.

To compare these two different modeling methods for a linearly tapered beam, a beam with nominal dimensions and A=0.75 inches and B=0.25 inches was studied. This corresponds to R=3. The number of elements was increased with each method until the zeros and poles converged. Table 4.3 presents the results from Method 1 where all elements were of equal length, and Table 4.4 presents the results from Method 2 where the end elements were half the length of all other elements. Although only two methods are considered in this research, there are many different ways to discretize a nonuniform link.

The two methods were evaluated based on an error function. When the tapered beam was modeled with 80 elements, both methods converged to nearly identical values for the poles and zeros. These values, when NE=80, were taken to be the "correct' values and other cases were compared to this case. The error, ε, was defined for the zeros as:

$$\varepsilon = \left| \frac{z_{80,i} - z_{NE,i}}{z_{80,i}} \right| \tag{4.2}$$

where i refers to the ith zero

A similar definition was used for the poles. The value of ε at the top of each column represents the maximum of all individual errors in each column. As the tables show, Method 2 provided better results for the same number of elements. In each table, one column was shaded to distinguish it as the number of elements needed to get the error under 1%. For Method 2, this column corresponded to NE=10 as opposed to NE=20 for Method 1. Thus, compensating the end elements did provide a better model of a linearly tapered beam, and this method was used in the following studies unless specified otherwise.

When comparing different link designs to evaluate pole/zero location as a function of link shape, it was

necessary to keep some parameter constant to aid in the evaluation. For a single-link manipulator rotating in the horizontal plane, the link's mass moment of inertia about its axis of rotation, I_y, was of importance. This parameter directly affected the dynamic equations of motion and was an important design parameter in terms of motor selection. In the following studies, several link designs were evaluated for a given value of I_y. A tapered link's moment of inertia about its axis of rotation in terms of the links parameters: L, A, B, H, and ρ is found to be:

$$I_y = \frac{\rho H}{48}(A^3 + A^2B + AB^2 + B^3 + 4AL^2 + 12BL^2) \tag{4.3}$$

For a given tapered link design, one can use Equation 4.3 to determine I_y. Knowing I_y, one can change the value of A and solve Equation 4.3 for B. Since the equation was cubic in B, the commercial package *Mathematica* was used to solve for B. Following this method, a group of tapered link designs were generated all with the same I_y.

The first study investigated several tapered link designs with nominal dimensions and all designs having I_y=764.05 in-lb-sec^2. Table 4.5 presents the raw data for each of these designs. Even with I_y held constant, it was still difficult to interpret the data. To aid in developing a relationship between zero location and link shape, the zeros were normalized with respect to the first pole for each design. The first pole is an important parameter in control system design, and normalizing the zeros with respect to the first pole aided in the interpretation of the results. Table 4.6 presents the normalized data for those designs with I_y=764.05 in-lb-sec^2. The second study presents data for several link designs with nominal dimensions and I_y=1528.1 in-lb-sec^2. Table 4.7 shows the raw data for these link designs and Table 4.8 shows the normalized data for these designs. Figures 4.4 and 4.5 show pole/zero maps for selected values of R for I_y=764.05 and I_y=1528.1 respectively.

Several patterns were evident by examining the raw data. First as a general rule, both the poles and zeros increased (moved away from the origin) as the taper on the beam increased. Increasing the taper effectively moved more of the link mass closer to the base. Increasing the value of the poles is often desirable to push them out of the system bandwidth and increase system response speed. The ordering of poles and zeros was the second pattern recognized. In a collocated system, the poles and zeros will both lie on the imaginary axis in complex conjugate pairs and in an alternating order. This means, along the imaginary axis, the poles and zero are found in the order p_1, z_1, p_2,z_2, etc. or vice versa. Previous research [18] has found this alternating order of poles and zeros does not hold for nonminimum phase systems. Referring to Table 4.5, notice the order of the magnitude of poles and zeros was: z_1,p_1,p_2,z_2,p_3,z_3,p_4,p_5,z_4.... p_2 jumped in front of z_2, and the same occurred for p_5. This reordering of poles and zeros can be critical as accurate knowledge of the pole/zero order is important for control system design.

Important information was learned from examining the relationship between the taper ratio, R, and the values of the normalized zeros. Figure 4.8 better illustrates this point showing both polynomial fits on the same graph. Even though the coefficients were different for each polynomial fit, the curves were nearly identical.

This illustrates an important relationship in the design of tapered links. For a given ratio R, the normalized zero will always remain the same. The designer can choose the location of the first pole and zero, determine the normalized zero, and then using Figure 4.8 find the appropriate taper ratio R. Of course there are constraints on this process. A ratio less than one corresponds to a taper with B greater than A, which is usually undesirable. At the other end, R is limited by the value of H. If A is larger than the value of H, the link will be wider at the base than it is tall, and the assumption that the link is stiff in the vertical plane will no longer be valid. Although the designer can choose the pole/zero relationship, the values of normalized zeros are limited to approximately 0.72-0.82 (according to Figure 4.8).

A simple verification of the above relationship is the uniform beam which has no taper. According to the stated relationship, the normalized first zero should be the same for all uniform beams. Table 4.9 presents the results for several uniform beam designs. All cases had nominal dimensions. The normalized zero in all cases was 0.726 which confirmed the normalized zero will not change as long as R is constant.

Previous studies demonstrated how the designer can choose the pole/zero relationship and then determine the appropriate taper design from the ZERO results. This study presents the designer with another freedom. Once the taper is chosen, the designer can change the link to independently adjust the value of I_y. Table 4.10 presents the results of a study performed on designs with L=40 inches, and all designs have the same taper. The height of the link was changed to adjust the value of I_y.

One should notice that the pole and zero locations of all designs in Table 4.10 were the same, yet the value of I_y changed with adjustments in link height. Since the adjustment of H is out of the plane of motion, it had no effect on the location of poles and zeros. Combining this with the results from the previous study, the designer can effectively choose the location of poles and zeros and independently adjust the links moment of inertia about its axis of rotation to meet the needs of the particular system.

CONCLUSIONS

Program ZERO was developed as a tool to locate the poles and zeros of a single-link manipulator modeled as a pinned-free Euler-Bernoulli beam. The program used transfer matrix theory to allow for variable cross-sections granting the designer new freedom in analysis of nonuniform link designs. The results were shown to be very accurate when system pole location was compared to analytic solutions for uniform beams. Several results from previous studies were confirmed with this research.

First, the reordering of poles and zeros was confirmed for nonminimum phase systems. Accurate knowledge of pole/zero order is critical for proper control system design. In conjunction with this, Tables 4.3 and 4.4 show that even for very few elements in the model, the program still predicts the proper order of poles and zeros.

Second, the studies presented suggested the nonminimum phase characteristics could not be eliminated by changing the structural design of the link. The system will be nonminimum phase above a finite frequency dictated by the location of the first nonminimum phase zero. It may be possible that this frequency is out of the operating range and not of concern to the designer.

The major contributions of this research are the development of the ZERO program to determine zero and pole location for a single-link nonuniform flexible manipulator, and formulation of a design procedure to place the first pole and zero and independently change the value of the link's moment of inertia about its axis of rotation to meet the needs of the system.

Program ZERO was set up specifically for pinned-free boundary conditions of the model and determines pole and zero location based on a frequency range entered by the user. Linearly tapered beams were studied in this research, but any type of nonuniform beam can be analyzed by program ZERO. Slight modifications would also allow for different boundary conditions.

The design procedure for tapered beams allows the designer to choose the first pole and zero subject to certain physical constraints. These physical constraints only allow for approximately 25% variation in R according to Table 4.6. This zero to pole ratio defines a particular taper ratio according to the collected data. Keeping the ratio the same, the size of the taper can be changed to get the proper magnitude of the pole and zero. With the pole and zero placed, the height of the beam can be changed to adjust the link's moment of inertia about its axis of rotation. This procedure can be used to design tapered links to meet the particular requirements of the system.

Program ZERO was designed to model a single-link manipulator modeled with pinned-free boundary conditions. This is a simplified model, but it was necessary to show transfer matrices yield good results for this case before progressing to more complicated problems. Now that transfer matrices have proven useful to solve for zero location, future work exists to extend the results of this research.

First, the program could be modified so the user could input the desired boundary conditions which best represent the system. This could include hub inertia or end-point mass. Second, the program could be extended to multi-link designs to predict pole and zero location for different configurations. Transfer matrices have been derived for rotary joints and many other elements. The DSAP package developed by Book, et. al. [6] handles multi-link models and would be a good reference. Finally, the results for tapered link designs could be applied to the inverse dynamic algorithm developed by Kwon and Book [9]. This method requires mode shapes for the assumed modes and uses pinned-pinned boundary conditions, which can also be found using transfer matrix techniques as shown in Book, et al.[6].

ACKNOWLEDGEMENTS

This work was performed with partial support from grant NAG 1-623 from the National Aeronautics and Space Administration. NASA bears no responsibility for its content.

BIBLIOGRAPHY

[1] Asada, H., Park, J.-H., and Rai, S., "A Control-Configured Flexible Arm: Integrated Structure/Control Design," *Proceedings of the 1991 IEEE International Conference on Robotics and Automation*, Sacramento, California, April, 1991, pp. 2356-2362.

[2] Bayo, E., "A Finite Element Approach to Control the End-Point Motion of a Single-Link Flexible Robot," *Journal of Robotic Systems*, Vol. 4, No. 1, 1987, pp.63-75.

[3] Beer, Ferdinand, and Johnson, Russell, Jr., *Vector Mechanics for Engineers, Statics and Dynamics*, Third Edition, McGraw-Hill, New York, 1977.

[4] Book, W. J., *Design and Control of Flexible Manipulator Arms*, Ph.D. Thesis, Massachusetts Institute of Technology, April, 1974.

[5] Book, W. J., and Kwon, D.-S., "Contact Control for Advanced Applications of Light Weight Arms," *Symposium on Control of Robots and Manufacturing*, Arlington, Texas, 1990.

[6] Book, W. J., Majette, M., and Ma, K., *The Distributed Systems Analysis Package (DSAP) and Its Application to Modeling Flexible Manipulators*, NASA Contract NAS 9-13809, Subcontract No. 551, School of Mechanical Engineering, Georgia Institute of Technology, 1979.

[7] Churchill, R. V., and Brown, J. W., *Complex Variables and Applications*, Fifth Edition, McGraw-Hill Publishing Company, New York, 1990.

[8] Kwon, D.-S., *An Inverse Dynamic Tracking Control for Bracing A Flexible Manipulator*, Ph.D. Dissertation, Georgia Tech, Woodruff School of Mechanical Engineering, June, 1991.

[9] Kwon, D.-S., and Book, W. J., "An Inverse Dynamics Method Yielding Flexible Manipulator State Trajectories," *Proceedings of the American Control Conference*, June, 1990, pp. 186-193.

[10] Majette, M., *Modal State Variable Control of a Linear Distributed Mechanical System Modeled with the Transfer Matrix Method*, Master's Thesis, Georgia Tech, Woodruff School of Mechanical Engineering, June, 1985.

[11] Meirovitch, L., *Elements of Vibrational Analysis*, McGraw-Hill, New York, 1986.

[12] Misra, Pradee, "On The Control of Non-Minimum Phase Systems," *Proceedings of the 1989 American Control Conference*, 1989, pp. 1295-1296.

[13] Nebot, E. M., Lee, G. K. F., and Brubaker, T. A., "Experiments on a Single Link Flexible Manipulator,", *Proceedings from the USA-Japan Symposium on Flexible Automation Crossing Bridges: Advances in Flexible Automation and Robotics*, 1988, pp. 391-398.

[14] Park, J.-H., and Asada, H., "Design and Analysis of Flexible Arms for Minimum-Phase Endpoint Control," *Proceedings of the American Control Conference*, 1990, pp. 1220-1225.

[15] Park, J.-H., and Asada, H., "Design and Control of Minimum-Phase Flexible Arms with Torque Transmission Mechanisms," *Proceedings of the 1990 IEEE International Conference on Robotics and Automation*, 1990, pp. 1790-1795.

[16] Pestel and Leckie, *Matrix Methods in Elastomechanics*, McGraw-Hill, New York, 1963.

[17] Rao, Singiresu S., *Mechanical Vibrations*, Addison-Wesley Publishing Company, Reading, Massachusetts, 1986.

[18] Spector, V. A., and Flashner, H., "Modeling and Design Implications of Noncollocated Control in Flexible Systems," *Journal of Dynamic Systems, Measurement, and Control*, Vol. 112, June, 1990, pp. 186-193.

[19] Spector, V. A., and Flashner, H., "Sensitivity of Structural Models for Noncollocated Control Systems," *Journal of Dynamic Systems, Measurement, and Control*, Vol. 111, December, 1989, pp. 646-655.